N-doping effects on the oxygen sensing of TiO_2 films

C. Buono, M. Desimone, F. Schipani, C. M. Aldao, C. I. Vignatti, C. I. N. Morgade, G. F. Cabeza & T. F. Garetto

Journal of Electroceramics

ISSN 1385-3449

J Electroceram
DOI 10.1007/s10832-017-0100-3

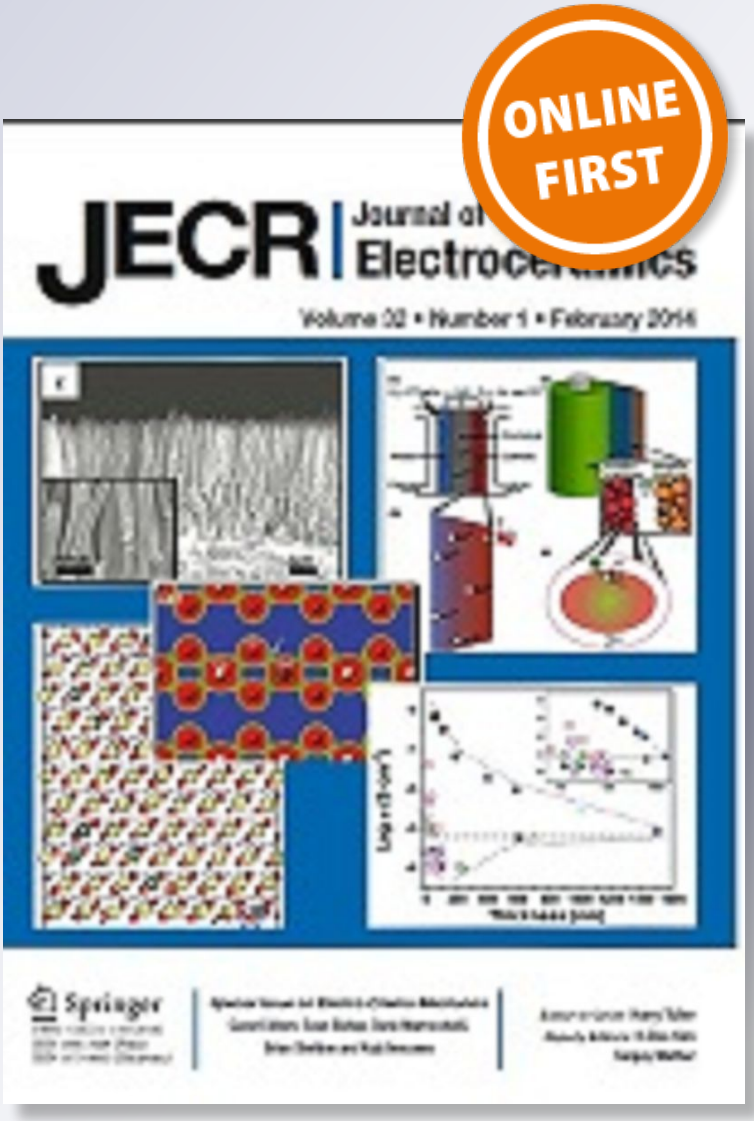

Springer

J Electroceram
DOI 10.1007/s10832-017-0100-3

N-doping effects on the oxygen sensing of TiO_2 films

C. Buono[1] · M. Desimone[1] · F. Schipani[1] · C. M. Aldao[1] · C. I. Vignatti[2] · C. I. N. Morgade[3,4] · G. F. Cabeza[4] · T. F. Garetto[2]

Received: 22 May 2017 / Accepted: 14 July 2017

Abstract Gas sensors based on Titanium dioxide films have been a subject of interest due to its high sensitivity and low cost. The sensing mechanism of this type of sensors is based on the conduction mechanism, which is governed by the potential barriers formed at the inter-grains of the polycrystalline structure. The shape of these potential barriers strongly depends on the characteristics of the material, and then it is expected that a doping aggregation will affect significantly the conductivity and thus the sensitivity of the sensor. In this work, we study the effect in the oxygen sensitivity of titanium dioxide films due to N-doping. We developed a model in order to explain our experimental results based on the fact that, for the particle size of our titanium dioxide samples, grains are completely depleted of carriers.

Keywords Polycrystalline semiconductors · Electrical conduction · Intergranular barriers · Tunneling

✉ C. Buono
Cbuono@mdp.edu.ar

[1] Instituto de Investigaciones en Ciencia y Tecnología de Materiales (INTEMA), Universidad Nacional de Mar del Plata-CONICET, Juan B. Justo 4302, B7608FDQ Mar del Plata, Argentina

[2] Grupo de Investigaciones en Ciencia e Ingeniería Catalíticas (GICIC), INCAPE, UNL-CONICET, CCT CONICET Santa Fe, Colectora Ruta Nac. 168, km 0, Paraje ″El Pozo″, (3000), Santa Fe, Argentina

[3] Universidad Tecnológica Nacional, 11 de Abril 461, B8000LMI Bahía Blanca, Argentina

[4] Grupo de Materiales y Sistemas Catalíticos, Instituto de Física del Sur (IFISUR), Departamento de Física, Universidad Nacional del Sur (UNS), CONICET, Av. Alem 1253-, B8000CPB Bahía Blanca, Argentina

1 Introduction

Metal-oxide semiconductor gas sensors can monitor the content of oxidizing and reducing gas molecules in a surrounding medium, which reflects in the resistance of a sensing film. Thus, a gas-sensing film and a substrate, including electrodes and heating elements, convert a chemical quantity into an electrical quantity for purposes of a measurement. This type of gas sensors has been subjected to extensive research due to low cost of production and wide range of applications, such as detection of flammable, toxic, and explosive gases [1–4].

Despite the advances in the field, the development of this type of sensors has been mostly built on empirical results [5–8]. Indeed, the gas-sensing mechanism remains not fully understood. It is usually accepted that the electrical conduction in polycrystalline semiconductors is dominated by intergranular potential barriers that have a Schottky-type nature. Oxide semiconductors, such as tin or titanium oxides, are usually oxygen-deficient and then they are of n-type. Crystallites of the semiconductor oxide film present a surface layer that is depleted of electrons. The width of this layer depends on the oxygen vacancy concentration and height of surface barriers. When the sensing material is exposed to a different atmosphere, surface reactions affect intergranular barriers leading to a change in conductance. Relevant issues to sensing include film structure, particle size, chemical composition, and thermal treatments of thick films.

Titanium dioxide has attracted great interest as it is found in a variety of applications in different fields, such as photocatalysis, photovoltaics, and gas sensors [8–12]. There are seven known and hypothetical Titanium dioxide polymorphs (anatase, rutile, columbite, baddeleyite, cotunnite, pyrite, and fluorite structures); nevertheless, in nature, Titanium dioxide presents three different forms, which in order of abundance, are rutile, anatase, and brookite. Anatase turns into

Published online: 26 July 2017

rutile above 400–600 °C and the temperature of this irreversible transformation decreases with increasing pressure [13]. Moreover, rutile is denser than anatase, so bulk rutile is considered to be stable with respect to bulk anatase, both at high temperature and high pressure. However, rutile is metastable concerning anatase when the Titanium dioxide particle size is below roughly 14 nm [14]. In particular, anatase is characterized by high electron mobility responsible for its elevated sensitivity and faster response as a gas sensor [15] and it has been successfully used in gas-sensing devices [16–22]. Akbar and co-workers discussed the electrical response of doped and undoped anatase gas sensors including the influence of several additives [23–25].

Here, we study the conductivity response to changes in the oxygen atmosphere content of a Titanium dioxide thick film. In particular, we compare the outcomes for samples with and without N-doping. The obtained results constitute a strong evidence for the doping contribution in the conductivity and sensitivity of polycrystalline semiconductor films.

2 Experimental details

Experimental analysis was carried out using a commercial undoped Titanium dioxide (Hombifine N, Sachtleben Chemie) and N-doped Titanium dioxide. The later was synthesized by precipitation method proposed by Wang et al. [26] using titanium (IV) isopropoxide $Ti(OCH(CH_3)_2)_4$ (Aldrich 97%) and concentrated nitric acid. The solution was stirred vigorously for 30 min and aqueous ammonium hydroxide solution (Cicarelli 28%) was added drop by drop until pH 9. The resultant precipitate was filtered, washed with deionized water and dried in air at room temperature. After that, the dried precipitate was calcined in air at 623 K for 4 h.

The crystalline structure and crystal size were determined with X-ray diffraction (XRD) in the range of $2\theta = 20–80°$ using a PANalytical X'Pert Pro diffractometer and Ni filtered Cu Kα radiation ($\lambda = 1.54$ Å). Crystallite sizes were calculated using the Scherrer eq. [27].

Raman spectra were acquired in a Renishaw In Via Reflex system equipped with a charge-coupled device (CCD) detector of 1040 × 256 pixels and coupled to a Leica microscope with a computer-controlled stage. An Argon laser line (514 nm) with a nominal power of 50 mW was used as excitation source, in combination with a grating of 2400 grooves/mm. The laser power was kept below 5% to avoid sample damage. A 50× (0.75NA) Leica metallurgical objective was used in the excitation and collection paths. Spectra were acquired in 1 s with at least 5 accumulations.

With different powders, pastes were prepared with an organic binder (glycerol). The used solid/organic binder ratio was ½, and no dopants were added. Thick, porous film samples were made by painting onto insulating alumina substrates on which electrodes with an interdigitated shape made by sputtering. A 96% dense alumina substrates were placed in a sputtering chamber and an adhesion layer consisting of 25 nm of titanium was deposited. Then, a platinum film 200 nm thick was then deposited over the Ti layer. Electrodes were defined using a 20 W laser. The interelectrode distance was 20 μm. After painting, in order to evaporate the organic binder and to improve the adhesion of films to the alumina substrate, samples were kept at 100 °C for 1 h in air. Later, samples were heated up to 380 °C using a heating rate of 1 °C/min and exposed to dry air at 380 °C during 1 h.

For gas-sensing measurements, the films were tested in a chamber with temperature, pressure, and gas composition control. Electrical resistance and impedance measurements were carried out with an Agilent 3440A multimeter and a HP4192A impedance analyzer, in the 20 Hz–10 MHz frequency range. Measurements were done under vacuum (10^{-4} atm) and in dry air at atmospheric pressure.

3 Results and discussion

The XRD patterns of pure Titanium dioxide and N-doped Titanium dioxide samples are presented in Fig. 1. The anatase phase has been retained without phase change after nitrogen doping. The line widths of the anatase (101) diffraction peak of the two samples were obtained by fitting the measured peaks by a mixed Lorenzian-Gaussian shape. Comparing results, one can see that pure Titanium dioxide and N-doped samples have almost the same crystallite size (~8–9 nm). Overall, the diffraction peaks of the pure sample are more intense than the N-doped Titanium dioxide powder, indicating that the pure powder has a better crystal quality.

Figure 2 shows the Raman spectra of the pure, and nitrogen-doped titanium dioxide. The observed Raman lines

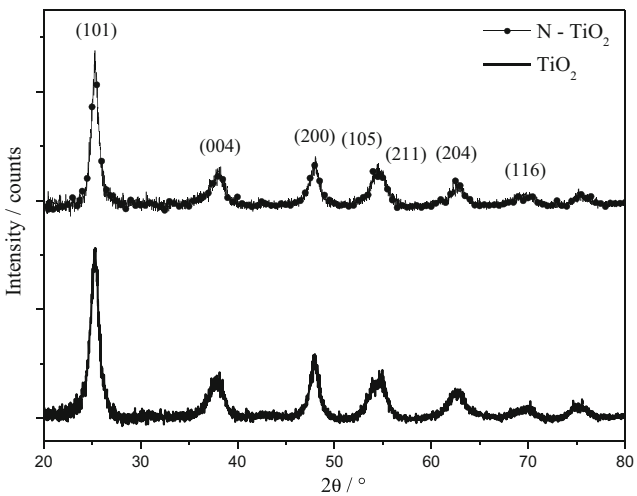

Fig. 1 XRD patterns of pure Titanium dioxide and N-doped Titanium dioxide samples

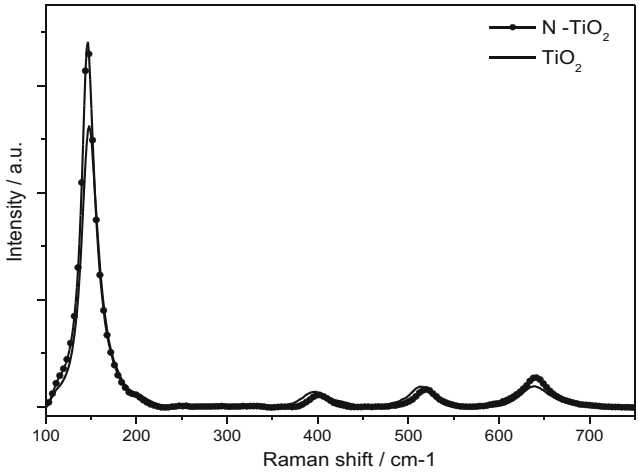

Fig. 2 Raman spectra of the pure and nitrogen-doped titanium dioxide

at 147, 398, 513 and 640 cm^{-1} can be assigned to the E_g, B_{1g}, A_{1g} and E_g modes of the anatase phase, respectively [28]. It can be seen that the Raman shift and the relative intensity of lowest-frequency E_g Raman mode is affected by doping. It is known that Raman lines become weak and broad when the samples have local lattice imperfections [29]. Since with nitrogen doping the intensity of the E_g mode increases, nitrogen must affect the Raman scattering efficiency.

To investigate the effect of nitrogen doping on the structure of the titanium dioxide, the Raman spectrum of N-doped Titanium dioxide was fitted, and the result is shown in Fig. 3. As can be seen, the peaks at 400, 518, and 638 cm^{-1} with a dash dotted line are the vibration peaks of anatase. In the fitting curves, two peaks at about 545 and 670 cm^{-1} with a dotted line can be observed distinctly, which are attributed to the vibration of Ti-N. According to previous reports, in the Raman spectrum, the band at 550 cm^{-1} is the first-order scattering of non-stoichiometric titanium nitride and the common component at 680–700 cm^{-1} is ascribed to second order scattering of non-stoichiometric titanium nitride [27, 30]. Typical

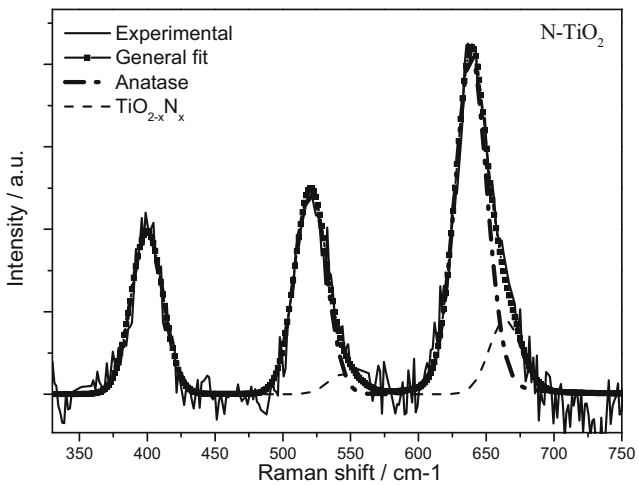

Fig. 3 Raman spectrum of N-doped Titanium dioxide fitting

vibrational bands of Ti-N can be found in the Raman spectrum of N-doped sample, indicating that nitrogen replaces some oxygen atoms in the titanium dioxide lattice.

In order to analyze the effect of the N-doping on the titanium dioxide sensitivity, we measured the resistivity of Titanium dioxide and N-doped Titanium dioxide films to atmosphere changes from air to vacuum and viceversa. Figure 4 shows three different stages (I, II and III), in the first stage, denoted as I, both samples (pure titanium dioxide and N-doped titanium dioxide) are exposed to air atmosphere at a temperature of T = 350 °C, held fixed in the three stages. In stage II, the chamber pressure was reduced to approximately 10^{-4} atm (referred here as vacuum), and then the resistivity of both samples decreases abruptly, as regularly observed in n-type metal-oxide semiconductors. In stage III samples are exposed again to air atmosphere; there is a quick increase of the electrical resistance, and then a steady increase for both types of studied samples, undoped and N-doped. This is expected due to the transfer of electrons from bulk to the surface as consequence of the interaction of oxygen with grain surfaces [30]. It is evident that the N-doped sample presents larger conductivity and sensitivity. The rapid increase of resistance in stage III could be attributed to the fast adsorption of oxygen at intergrains, due to the open porous microstructure, while the subsequent evolution could be related with a significant diffusion of oxygen into the grains. From these processes, the barrier height and the depletion width become larger and, as a consequence, the sample resistance increases.

At temperatures greater than ~200 °C, oxygen diffusion into the grains is possible, with the consequent annihilation of oxygen vacancies. Conversely, if oxygen diffuses out of the

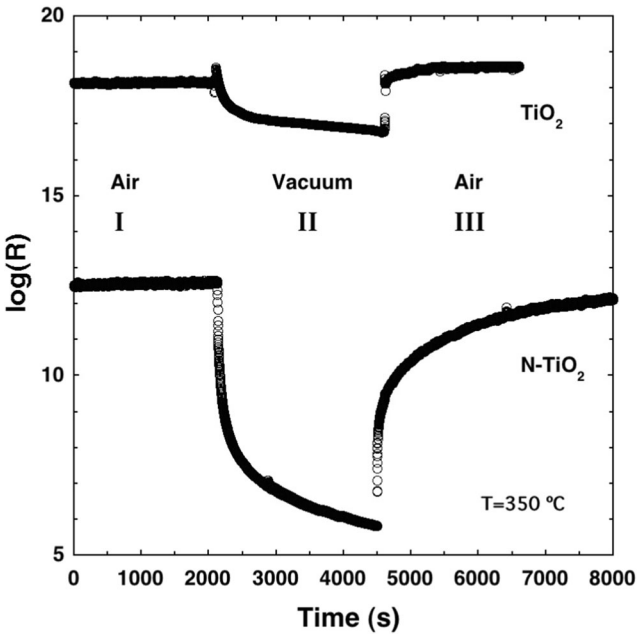

Fig. 4 Electrical resistance under vacuum and air exposure for undoped and N-doped titanium dioxide

grains, vacancies are generated. The adsorbed oxygen changes to various oxygen anion species transferring an electron form the oxide to the chemisorbed oxygen according the following processes [30, 31]

$$O_{2(gas)} \leftrightarrow O'_{2(ads)} \leftrightarrow O'_{ads} \leftrightarrow O''_{ads} \leftrightarrow O''_i \leftrightarrow O_O^{\times} \quad (1)$$

where $O_{2(gas)}$ refers to oxygen in the gas environment, $O_{2(ads)}$ to an oxygen molecule adsorbed at the grain surfaces, O'_{ads} and O''_{ads} to singly and doubly ionized monatomic oxygen at the grain surface, O''_i to interstitial oxygen, and $O_O^{\times}$ to oxygen at the titanium dioxide lattice. The interstitial oxygen O''_i migrates from the surface to the bulk annihilating oxygen vacancies, as follow:

$$V_O^{\bullet\bullet} + O''_i \leftrightarrow O_O^{\times} \quad (2)$$

Then, for temperatures greater than ~200 °C by exposing the sample to an oxygen rich atmosphere, a decrease in $V_O^{\bullet\bullet}$ can be expected. Conversely, under vacuum $V_O^{\bullet\bullet}$ is expected to increase.

If the particle size were much larger than the width of the surface layer, the charge depletion would occur in a relatively reduced surface region of the particle. On the contrary, in a small particle, it can happen that its diameter is such that the whole crystallite is depleted of electrons and then the electrical conduction mechanisms are different. Since the gas sensing is based on the change of electrical resistance that follows a change in the gas atmosphere, the sensor response is expected to directly depend on the grain size.

In order to check the depletion of the crystallite in the titanium dioxide, we first determined the capacitance of the films under vacuum and air at 1 MHz, a frequency at which the contribution of traps can be disregarded [31]. Experimentally we found that, the capacitance before the incorporation of the sensor film for 1 MHz is 12 pF. In order to analyze the film capacitance, it is necessary to consider the shape of the used electrodes. After the incorporation of the film, the capacitance becomes ≈ 35.5 pF. The contribution to the total capacitance due to the film of thick b_{film}, can be expressed, as a good approximation [32],

$$C_{film} = \frac{\varepsilon_0 \varepsilon_r}{\pi} l. \left[\sinh^{-1}\left(b_{film} \Big/ a \right) + 0.234 \right] \quad (3)$$

where l is the length of the electrode, $2a$ is the width of the inter-electrode pathway and ε_r is the film relative permittivity. For our set-up $l = 11$ cm, $a = 10$ μm, $b_{film} = 0.09$ mm and $C_{film} = 35.5$ pF – 12 pF = 23.5 pF. With the above information we can determine the film permittivity $\varepsilon_r \approx 24$, which is consistent with reported values for the anatase permittivity at 1 MHz [33].

If we assume a spherical grain, the condition for which grains become completely depleted is [31]

$$V_s = \frac{eN_d R^2}{6\varepsilon_0 \varepsilon_r} \quad (4)$$

where V_s is the band bending, R the grain radius, N_d the oxygen vacancies concentration, e the electron charge, ε_0 the vacuum permittivity, and ε_r the relative permittivity. Typical values of band bending goes from 0.6 eV up to 1 eV; therefore, by using $V_s = 0.6$ eV, we can estimate the lower limit for the complete depletion to occur. Thus, using $R = 4.25$ nm (half of crystallite size average obtained from Raman spectroscopy and XRD) and $\varepsilon_r \approx 24$, we get that $N_d \leq 2.6 \times 10^{26}$ m^{-3}. This is an extremely large vacancy concentration.

The above results and considerations imply that, for the particle size of our titanium dioxide samples, grains are completely depleted of carriers. After the exposure to vacuum, diffusion from the bulk of the grains to the intergrains can take place. If barriers reduce to the point at which quasi-neutral regions at the grains centers develop, the capacitance should increase. However, we observe a slight reduction in capacitance that we attribute to an increase in the film porosity. Thus, driven by the above analysis, we consider that grains continue being completely depleted of carriers.

According to the results of Fig. 4, the larger conductivity and sensitivity of N-doped samples can be explained with two different models, taking into account two different main mechanisms of conduction, as depicted in Fig. 5 or Fig. 6. In these figures, (a) and (b) refer to pure anatase under air and vacuum, respectively; while (c) and (d) refer to N-doped anatase under air and vacuum, respectively.

In one hand, most researchers assume that electrical conduction is dominated by thermionic emission [8]. If this were

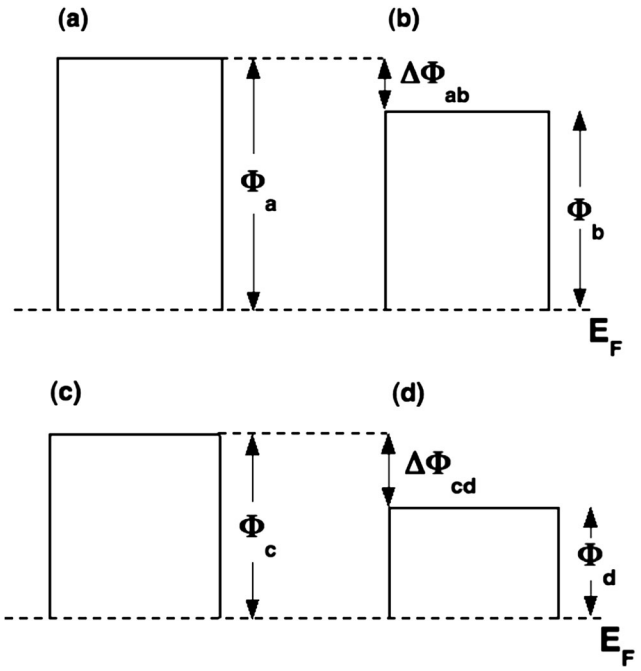

Fig. 5 Expected band bending changes assuming thermionic emission as the dominant conduction mechanism. (**a**) and (**b**) refers to pure titanium dioxide under air and vacuum, respectively; while (**c**) and (**d**) refers to N-doped titanium dioxide under air and vacuum, respectively

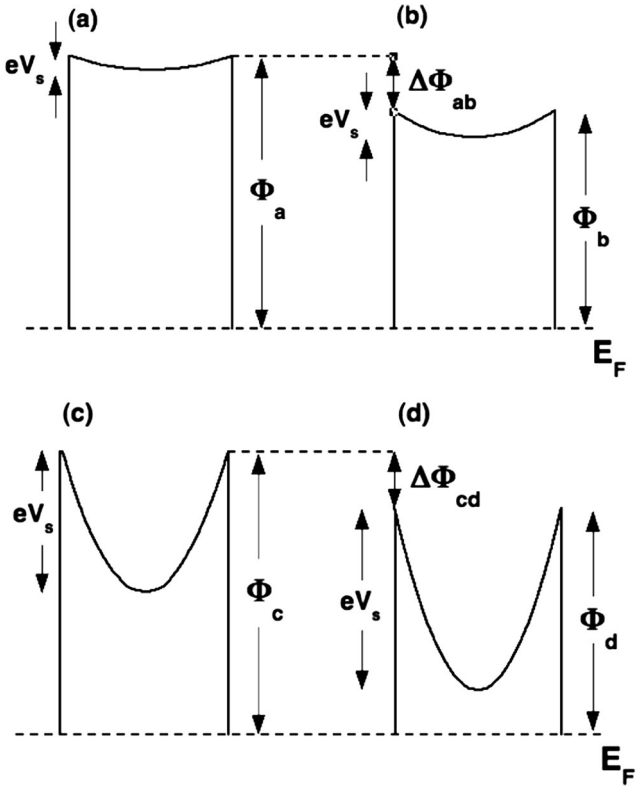

Fig. 6 Possible band bending changes assuming tunneling contribution as the dominant conduction mechanism. (**a**) and (**b**) refers to pure titanium dioxide under air and vacuum, respectively; while (**c**) and (**d**) refers to N-doped titanium dioxide under air and vacuum, respectively

the case, then barrier heights should behave as seen in Fig. 5. Resistances reported in Fig. 4 indicate that $\Phi_a > \Phi_b > \Phi_c > \Phi_d$. Also, since the sensitivity for the N-doped sample is larger, $\Delta\Phi_{cd} > \Delta\Phi_{ab}$. This analysis implies that nitrogen plays a crucial role at the surface of the grains. Indeed, not only reduces the intergranular barriers but also makes barriers more sensitive to changes in the environment.

On the other hand, other possible mechanism that can be responsible for the experimental findings is related to band bending, which can make relevant the tunneling contribution to the sample conductivity. In this case, Fig. 6, barriers corresponding to samples under air are considered having the same height, $\Phi_a = \Phi_c$. Also, barrier corresponding to samples under vacuum present the same height, $\Phi_b = \Phi_d$. If this were the case, the found differences in conductivity would depend on the sample doping. In the pure sample, the oxygen vacancy concentration is not very high and vacuum favors oxygen vacancies slightly increasing the band bending. If this takes place, tunneling can play a role in conductivity as electrons might tunnel the resulting intergranular barriers. It is known that nitrogen favors the oxygen vacancy formation and then the sample doping [34]. If so, a larger doping can be responsible for a larger band bending and then a more relevant contribution of tunneling through barriers. In this case, changes in conductivity could be explained as the result of different contributions of tunneling to conductivity. It is possible that both phenomena, barrier height and width changes, were present and responsible for the observed results.

4 Conclusions

In summary, we have studied and analyzed the resistivity of undoped and N-doped titanium dioxide under air atmosphere and vacuum and its sensitivity. We found that, for the N-doped sample, there is a significantly global decrease in the resistivity and the sensitivity to oxygen exposure is highly favored. In order to explain our experimental results, we determined the size of the crystallites of our samples through XRD and found that for the small particle sizes of our samples with a completely depleted grains must be the regular situation. We propose two different alternatives to explain the behavior of the sensitivity of the samples given that total grain depletion occurs. In the first one, the thermionic emission is the dominant conduction mechanism, electrons must jump over the potential barriers. In the second one, tunneling current is considered as the dominant contribution to electrical conduction trough the crystallite. Either of the two models, or a combination between them, could explain the difference in the sensitivity of the undoped and the N-doped titanium dioxide having into account that nitrogen favors the oxygen vacancy formation. The correct choice of the model will depend on the exact conduction mechanism of this type of sensors that must be deeply studied in future works.

Acknowledgements This work was partially supported by the National Council for Scientific and Technical Research (CONICET) of Argentina and the National University of Mar del Plata (Argentina).

References

1. M.J. Madou, R. Morrison, *Chemical Sensing with Solid State Devices* (Academic, San Diego, 1989)
2. N. Yamazoe, Sensors Actuators B Chem. **108**, 2–14 (2005)
3. N. Barsan, D. Koziej, U. Weimar, Sensors Actuators B Chem. **121**, 18–35 (2007)
4. I.-D. Kim, A. Rothschild, B.H. Lee, D.Y. Kim, S.M. Jo, H.L. Tuller, Nano Lett. **6**, 2009–2013 (2006)
5. N. Barsan, U. Weimar, J. Electroceram. **7**, 143–167 (2001)
6. M.A. Ponce, C. Malagu, M.C. Carotta, G. Martinelli, C.M. Aldao, J. Appl. Phys. **104**, 054907 (2008)
7. M.A. Ponce, M.S. Castro, C.M. Aldao, J. Mater. Sci.: Mater. Electron. **20**, 25–32 (2009)
8. W. Gopel, K. Schierbaum, Sensors Actuators B Chem. **26**, 1–12 (1995)
9. A. Werner, A. Roos, Sol. Energy Mater. Sol. Cells **91**, 609–615 (2007)
10. B. O'Regan, M. Grätzel, Nature **353**, 737–739 (1991)
11. C. Burda, Y. Lou, X. Chen, A.C. Samia, J. Stout, L. Gole, Nano Lett. **3**, 1049–1051 (2003)

12. H. Tang, K. Prasad, R. Sanjinés, F. Levy, Sensors Actuators B Chem. **26–27**, 71–75 (1995)
13. E.F. Osborn, J. Am. Ceram. Soc. **36**, 147–151 (1953)
14. S.J. Smith, R. Stevens, S. Liu, G. Li, A. Navrotsky, J. Boerio-Goates, B.F. Woodfield, Am. Mineral. **94**, 236–243 (2009)
15. M. Epifani, A. Helwig, J. Arbiol, R. Díaz, L. Francioso, P. Siciliano, G. Mueller, J.R. Morante, Sensors Actuators B Chem. **130**, 599–608 (2008)
16. L.A. Harris, J. Electrochem. Soc. **127**, 2657–2662 (1980)
17. E. Traversa, M.L. Di Vona, S. Licoccia, M. Sacerdoti, M.C. Carotta, M. Gallana, G. Martinelli, J. Sol-Gel Sci. Technol. **19**, 193–196 (2000)
18. I.-D. Kim, A. Rothschild, D.-J. Yang, H.L. Tuller, Sensors Actuators B Chem. **130**, 9–13 (2008)
19. B. Karunagaran, P. Uthirakumar, S.J. Chung, S. Velumani, E.-K. Suh, Mater. Charact. **58**, 680–684 (2007)
20. M.R. Mohammadi, D.J. Fray, M.C. Cordero-Cabrera, Sensors Actuators B Chem. **124**, 74–83 (2007)
21. D. Mardare, N. Iftimie, D. Luca, J. Non-Cryst. Solids **354**, 4396–4400 (2008)
22. A. Al-Homoudi, J.S. Thakur, R. Naik, G.W. Auner, G. Newaz, Appl. Surf. Sci. **253**, 8607–8614 (2007)
23. L.D. Birkefeld, M.A. Azad, S.A. Akbar, J. Am. Ceram. Soc. **75**, 2964–2968 (1992)
24. A.M. Azad, L.B. Youdunan, S.A. Akbar, M.A. Alim, J. Am. Ceram. Soc. **77**, 481–486 (1994)
25. P.K. Dutta, A. Ginwalla, B. Hogg, B.R. Patton, B. Chwieroth, Z. Liang, P. Gouma, M. Mills, S. Akbar, J. Phys. Chem. B **103**, 4412–4422 (1999)
26. J. Wang, W. Zhu, S. Liu, J. Phys. Chem. C **111**, 1010–1014 (2007)
27. Y. Cong, J. Zhang, F. Chen, M. Anpo, J. Phys. Chem. C **111**, 6976–6982 (2007)
28. W.F. Zhang, Y.L. He, M.S. Zhang, Z. Yi, Q. Chen, J. Phys. D. Appl. Phys. **33**, 912–916 (2000)
29. A.L. Bassi, D. Cattaneo, V. Russo, C.E. Bottani, E. Bartoriri, T. Mazza, P. Pisen, P. Midani, F.O. Ernst, K. Wegner, S.E. Pratsinis, J. Appl. Phys. **98**, 074305 (2005)
30. M. Batzill, U. Diebold, Prog. Surf. Sci. **79**, 47–154 (2005)
31. F. Schipani, M.A. Ponce, E. Joanni, F.J. Williams, C.M. Aldao, J. Appl. Phys. **116**, 194502 (2014)
32. Z.-W. Chen, C.-H. Shek, C.M. Lawrence Wu, J.K.L. Lai, Front. Mater. Sci. **7**, 203 (2013)
33. L. Zhou, R.C. Hoffmann, Z. Zhao, J. Bill, F. Aldinger, Thin Solid Films **516**, 7661–7666 (2008)
34. M. Batzill, E. Morales, U. Diebold, Phys. Rev. Lett. **96**, 26103 (2006)